Design of a Shack Hartmann Wavefront Sensor

January 11, 2017

Introduction

Atmospheric seeing quality is an important aspect for the performance of astronomical observatories. A valuable tool for assessing atmospheric seeing is the Shack Hartmann wavefront sensor, which is able to characterize the optical wavefront incident to an observatory telescope. This paper describes the design of a Shack Hartmann sensor whose application is to measure the optical aberrations of atmospheric turbulence that are seen by amateur observatories. The goal of the turbulence measurements is to provide insight for cost effective turbulence compensation, subject to the cost constraints of amateur observers.

Design of the Optical Beam Train

Referring to Figure 1 below, the Shack Hartmann sensor appends to the observing telescope, with the telescope's objective lens/mirror as the first element L_1 of an optical relay pair L_1, L_2 that concentrates the incoming light into a narrow beam, thereby reimages the telescope's aperture onto a small square lenslet array L_3. A second relay pair L_4, L_5 reimages the lenslet array spots onto a CCD focal plane chip. Pixel signals from the CCD focal plane image pass into a laptop computer via an Ethernet port to form movie frames of lenslet spot positions that are then analyzed by Matlab algorithms.

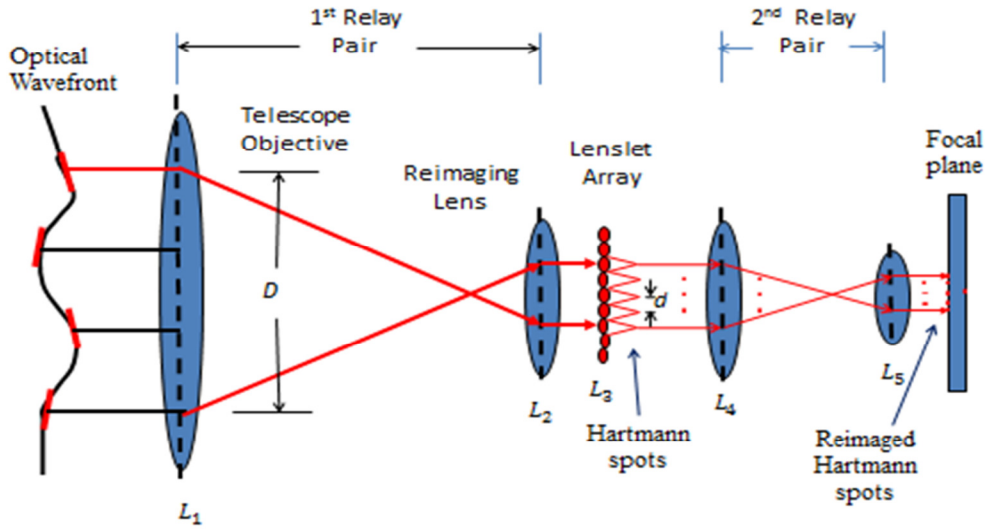

Figure 1 Optical beam train of the Shack Hartmann sensor.

The entrance pupil is this amateur's telescope aperture of 0.5 meters. The CCD focal plane is a 120 fps Point Grey Flea 3 camera that uses a 0.3 MP Sony ICX618 chip with a 648x488 array of 5.6 micron pixels. The design of the Shack Hartmann sensor begins with the selection of its lenslet array L_3. Once selected, the remaining optical design interfaces the lenslet array to the telescope's entrance aperture L_1 and to the CCD focal plane, respectively. All relay optics are achromats to minimize optical distortion.

The lenslet array design proceeds by first dividing the usually circular telescope aperture with diameter D into a usually square grid of subapertures with sides of dimension d. The number n of subapertures with sides d spanning the aperture diameter D are $n = D/d$. Within a sub aperture, wavefront phase models as a piecewise constant slope, i.e., local tip/tilt. Viewed as an aperture cross section, the subaperture length d is chosen to give a good straight line piecewise approximation to the continuous aberration within the aperture diameter D. A smaller d gives a better approximation, while a larger d risks the straight line assumption of constant sub aperture phase slope.

An optical relay system maps its input and output beams. Correspondingly, the first relay pair maps each subaperture location to lenslet location. Since the first relay pair provides this one-to-one mapping of sub aperture to individual lenslet, the number n of sub apertures across the telescope's aperture diameter defines the $n \times n$ lenslet array size.

For atmospheric turbulence, a measure of wavefront phase variation is given by the Fried coherence length r_o, which is defined as an air column diameter whose rms wavefront aberration is one radian. A conventional approach to array design makes $d = r_o$, so that $n = D/r_o$ is the number of coherence lengths across the aperture D. To guarantee that the subaperture piecewise constant slope approximation gives a valid wavefront representation, the smallest anticipated value of r_o defines n.

Apart from using a Shack Hartmann sensor, an easy way to estimate r_o is to record movies of angular star jitter about a star's average angular position from zenith. Using Fried's experession [1] for star jitter

$$\sigma^2 = 0.18\lambda^2 D^{-1/3} r_o^{-5/3}$$

and solving for r_o gives,

$$r_o = \left(\frac{0.18\lambda^2}{\sigma^2 D^{\frac{1}{3}}} \right)^{\frac{5}{3}}$$

for a telescope of diameter D, and optical wavelength λ, for which a mid-value of 0.5 microns (green light) is a good choice for a star light's visible wavelength band of 0.4 to 0.7 microns.

Measured r_o varies considerably over short time intervals. At this author's observatory $r_o$momentarily ranges from a minimum of 3 to 4 cm, to a maximum of 10 to 15 cm for the strongest to weakest atmospheric turbulence, respectively. For comparison, well located professional observatories have r_o values typically greater than 15 cm**.**

Note that the lenslet's $n \times n$ array size is a compromise. On one hand, a sufficiently large number of sub apertures needs to faithfully approximate the atmospheric turbulence perturbations

incident to the telescope's aperture with a sequence of straight line segments. On the other hand, astronomical subapertures are usually photon starved, with the telescope aperture star photon flux divided by the number of sub apertures. For subapertures of size $r_o \times r_o$ the ratio of subaperture area to total aperture is $r_o^2/A_{tot} = 4/\pi n^2$. Thus there is an immediate n^2 tradeoff between faithful piecewise wavefront approximation and the Shack Hartmann sensor's ability to measure turbulence using faint stars. Placing sensors on high mountain tops makes for S-H designs of greater photon sensitivity because r_o is larger and designed n is correspondingly less.

Additionally, the sensor's wavefront phase sensitivity also is inversely related to n^2 and diminishes strongly with increased n. The incremental positional change of the lenslett blur spot upon its focal plane blur spot is,

$$\left(\frac{\Delta\_blur\_spot\_pstn}{\Delta\_wavefront\_tilt}\right) = \left(\frac{telescope\_aperture}{n \times lenslet\_pitch}\right) \times (lenslet\_fl) \times \left(\frac{focal\_plane\_image\_height}{n \times lenslet\_pitch}\right)$$

The first term in parenthesis to the right of the equal sign follows from the Lagrange invariant and is the angular magnification, denoted M_1, of the first relay pair that reimages the telescope's larger aperture to the smaller beam size of the lenslet array. The denominator term, $n \times lenslet\_pitch$, is the diameter of the first relay pair's exit beam.

The last parenthetical term in the above expression is the magnification of the second reimaging lens pair and is denoted $1/M_2$ with $M_2 = n \times lenslet\_pitch/focal\ plane\ image\ height$. This reimaging magnification scales the mapping of the lenslet array's Hartmann's spots onto the focal plane. Since the exit beam appears in the denominator of both parenthetic terms, increasing the first relay pair's second lens exit beam diameter exacts a high price in wavefront tilt detection sensitivity, and hence this beam diameter should be small.

Dividing the worst measured r_o of 3 cm into the telescope's 50 cm aperture diameter and rounding gives the n x n lenslet array size as 17 x 17. AOA Xynetics, a subsidiary of Northrup Grumman, offers standard, off-the-self monolithic lenslet modules (arrays) with lenslet spacings ranging from 0.1 to 1.75 millimeter spacings, and focal lengths ranging from 0.5 to 260 millimeters. The Table 1 Excel spreadsheet below enumerates these selections and calculates magnification M_1, (column J), Lens2 focal length (column K), M_2 (column N), and wavefront tilt angle sensitivity (column O). The chosen lenslet array, sixth line from the top, in red, with a lenslet diameter of 190 microns and 10 mm focal length is chosen because it has good sensitivity (column O) of 5.37 microns/arc-sec, and a reasonable design requirement for M_2.

Interestingly, a greater sensitivity of 8.60 is achieved with a 400 micron diameter, 71 mm focal length lenslet, making the relayed beam diameter from L_2 twice as large, which by itself reduces sensitivity by $2^2 = 4$X. The loss in sensitivity is more than regained, however, by a focal length that is seven times longer. The lenslet's Airy disk diameter of 238 microns (column E) is a concern, however, as well as the larger M_2 of the 2nd relay system, which may necessitate the 2nd relay system consisting of two cascaded stages.

Lenslett Spacing (microns)	Focal Length (mm)	Lenslet F#	Lenslet Airy Disk (mm)	Number of Lenslets	Lenslett Array Height (mm)	Telescope Diameter (mm)	Telescope Fcl Length (mm)	First Relay DeMagnificatior	Relay Lens Fcl Length (mm)	Displacement/arc-sec at Lenslet Fcl Length (microns)	CCD Focal Plane Image (mm)	DeMagnification Lenslet to CCD Focal Plane	Displacement/arc-se at CCD (microns)	Focal Plane Airy Disk (mm)
(B)	(C)	(D)	(E)	(F)	(G)	(H)	(I)	(J)	(K)	(L)	(M)	(N)	(O)	(P)
		1000*D/B	2.44*0.00055*D		B*0.001*F			H/G	(G/H)*1	0.000005*(H/G)*C*1000	0.0056*400	G/M	L*(M/G)	E/N
100	0.5	5.0	0.0067	17	1.7	500	4160	294.1	14.1	0.74	2.24	0.76	0.97	0.009
100	1.1	11.0	0.0148	17	1.7	500	4160	294.1	14.1	1.62	2.24	0.76	2.13	0.019
100	1.7	17.0	0.0228	17	1.7	500	4160	294.1	14.1	2.50	2.24	0.76	3.29	0.030
125	1	8.0	0.0107	17	2.125	500	4160	235.3	17.7	1.18	2.24	0.95	1.24	0.011
188	8	42.6	0.0571	17	3.196	500	4160	156.4	26.6	6.26	2.24	1.43	4.39	0.040
190	10	52.6	0.0706	17	3.23	500	4160	154.8	26.9	7.74	2.24	1.44	5.37	0.049
200	1	5.0	0.0067	17	3.4	500	4160	147.1	28.3	0.74	2.24	1.52	0.48	0.004
200	6.3	31.5	0.0423	17	3.4	500	4160	147.1	28.3	4.63	2.24	1.52	3.05	0.028
203	5.8	28.6	0.0383	17	3.451	500	4160	144.9	28.7	4.20	2.24	1.54	2.73	0.025
203	6.5	32.0	0.0430	17	3.451	500	4160	144.9	28.7	4.71	2.24	1.54	3.06	0.028
203	7.8	38.4	0.0516	17	3.451	500	4160	144.9	28.7	5.65	2.24	1.54	3.67	0.033
250	1	4.0	0.0054	17	4.25	500	4160	117.6	35.4	0.59	2.24	1.90	0.31	0.003
250	18	72.0	0.0966	17	4.25	500	4160	117.6	35.4	10.59	2.24	1.90	5.58	0.051
250	19	76.0	0.1020	17	4.25	500	4160	117.6	35.4	11.18	2.24	1.90	5.89	0.054
300	3	10.0	0.0134	17	5.1	500	4160	98.0	42.4	1.47	2.24	2.28	0.65	0.006
300	7.6	25.3	0.0340	17	5.1	500	4160	98.0	42.4	3.73	2.24	2.28	1.64	0.015
312.5	34	108.8	0.1460	17	5.3125	500	4160	94.1	44.2	0.02	2.24	2.37	0.01	0.062
325	18	55.4	0.0743	17	5.525	500	4160	90.5	46.0	8.14	2.24	2.47	3.30	0.030
328	24	73.2	0.0982	17	5.576	500	4160	89.7	46.4	10.76	2.24	2.49	4.32	0.039
400	3.2	8.0	0.0107	17	6.8	500	4160	73.5	56.6	1.18	2.24	3.04	0.39	0.004
400	24	60.0	0.0805	17	6.8	500	4160	73.5	56.6	8.82	2.24	3.04	2.91	0.027
400	53	132.5	0.1778	17	6.8	500	4160	73.5	56.6	19.49	2.24	3.04	6.42	0.059
400	71	177.5	0.2382	17	6.8	500	4160	73.5	56.6	26.10	2.24	3.04	8.60	0.078
417	45	107.9	0.1448	17	7.089	500	4160	70.5	59.0	15.87	2.24	3.16	5.01	0.046
500	30	60.0	0.0805	17	8.5	500	4160	58.8	70.7	8.82	2.24	3.79	2.33	0.021
500	45	90.0	0.1208	17	8.5	500	4160	58.8	70.7	13.24	2.24	3.79	3.49	0.032
600	6.3	10.5	0.0141	17	10.2	500	4160	49.0	84.9	1.54	2.24	4.55	0.34	0.003
600	40	66.7	0.0895	17	10.2	500	4160	49.0	84.9	9.80	2.24	4.55	2.15	0.020
768	6.5	8.5	0.0114	17	13.056	500	4160	38.3	108.6	1.24	2.24	5.83	0.21	0.002
768	86	112.0	0.1503	17	13.056	500	4160	38.3	108.6	16.47	2.24	5.83	2.83	0.026
800	7.5	9.4	0.0126	17	13.6	500	4160	36.8	113.2	1.38	2.24	6.07	0.23	0.002
1000	17	17.0	0.0228	17	17	500	4160	29.4	141.4	2.50	2.24	7.59	0.33	0.003
1000	55	55.0	0.0738	17	17	500	4160	29.4	141.4	8.09	2.24	7.59	1.07	0.010
1060	260	245.3	0.3292	17	18.02	500	4160	27.7	149.9	36.07	2.24	8.04	4.48	0.041
1750	70	40.0	0.0537	17	29.75	500	4160	16.8	247.5	5.88	2.24	13.28	0.44	0.004
1750	90	51.4	0.0690	17	29.75	500	4160	16.8	247.5	7.56	1.12	26.56	0.28	0.003

Table 1 Selection of Lenslet array.

A Matlab based ray trace of the beam train using 3 x 3 ray matrices [2] was developed and is shown in Figure 2. Three ray bundles enter the telescope aperture, L_1 one along the optical axis, and two from opposite sides of a telescope aperture's diameter. Each of the three ray bundles has three rays, a ray with no tilt, a ray with tilt of plus one arc-second, and a ray with tilt of minus one arc-second. The three ray bundles are reimaged at L_2 and propagate to the 17 x 17 lenslet array, L_3 . Only three of the 289 lenslets are shown. The rays propagate beyond the lenslet array, with the three components of each ray bundle now being very apparent. The nine rays are then relayed with Lens 4 and 5 and are reimaged on the CCD focal plane.

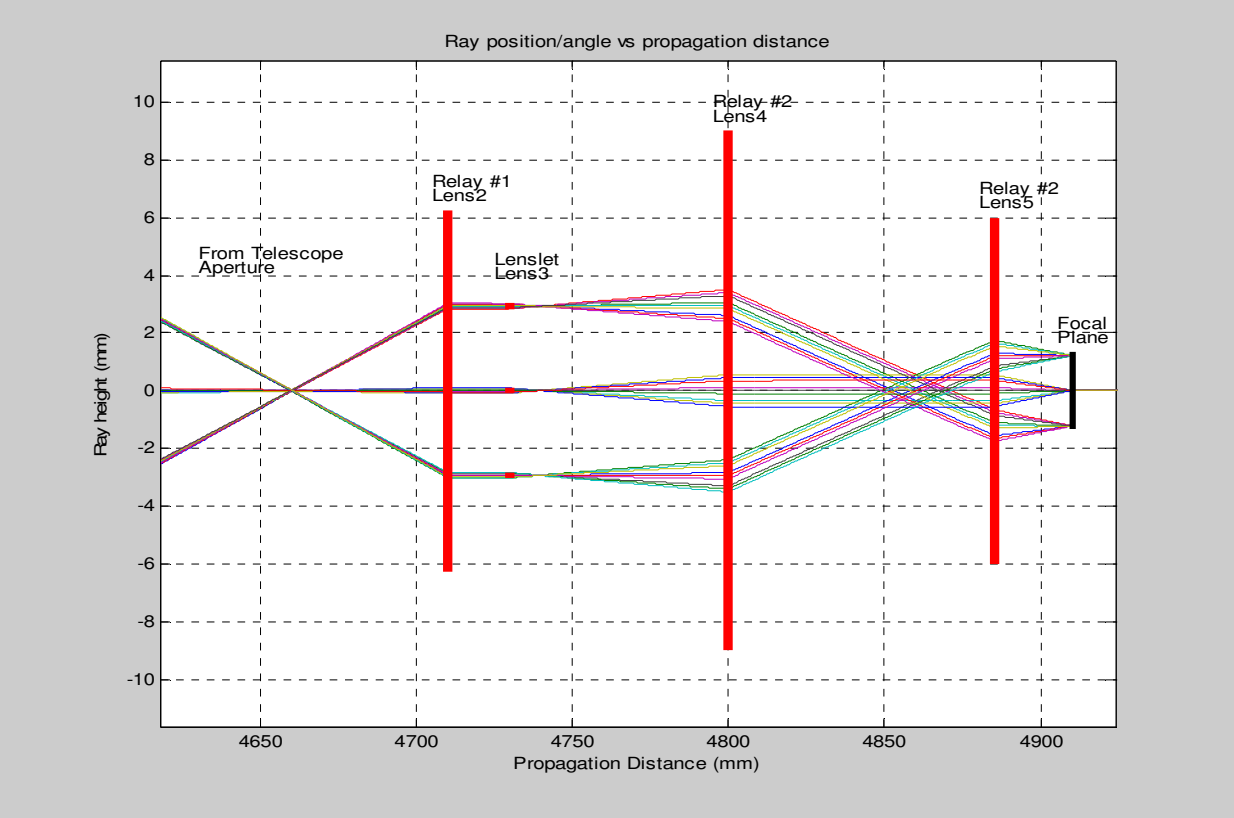

Figure 2 Shack Hartmann ray trace diagram. Three bundles, each consisting of three rays with -1, 0, 1 arc-sec diviation enter from the telescope aperture L_1. Lens L_2 reimages the columnated incoming rays to $L_1$and propagates them to the lenslet array L_3. The Hartmann spots from L_3 propagate through Relay #2 lenses L_2, L_5 and are reimaged at the focal plane. As a double check of Relay #2, note that the distance from front focal length

Note from Figure 2 that the conditions for an optical relay are satisfied as shown by the ray trace of Relay #2. The object (Hartman spots) distance to L_4 is the same distance as the L_4 focal distance, that the distance between L_4 and L_5 is the sum of the two focal lengths, and that the focal plane is at the L_5 focal distance.

Figure 3 shows the resultant lenslet blur spot image. It is seen that the blur spots are circular, indicating that each sub aperture's aberrations of order beyond tip/tilt are small and the wavefront is well represented by piecewise two dimensional straight line segments. Higher order aberrations would

otherwise produce distorted blur spots. Additionally, Figure 2 shows that there are no focal plane blur spots in the image center due to the telescope's secondary mirror casting its shadow on the telescope's primary. Between shadowed and illuminated regions some lenslets are only partially illuminated and in these transition region tip/tilt perturbation and scintillation makes the lenslet illumination time varying, which in turn makes the blur spots momentarily appear and disappear. Atmospheric scintillation also plays across the remaining face of the telescope aperture and produces deep fades in the illuminated lenslets. Accommodating these deep fades makes the image processing algorithm more challenging.

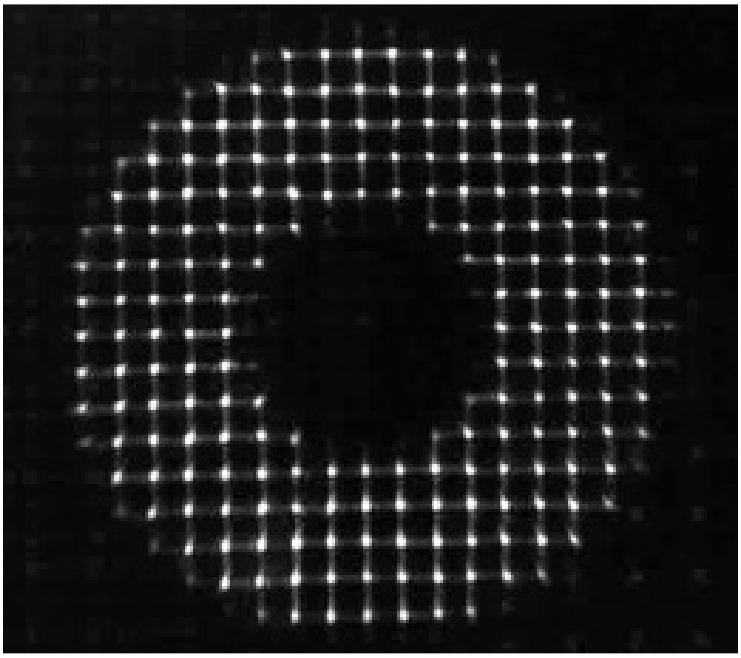

Figure 3 A 17×17 array of Hartmann spots. The center subapertures are in the shadow of the telescope's secondary mirror, are not illuminated, and appear dark. Similarly, subapertures outside the aperture also not illuminated, and are dark. The result is a "donut" like appearance of Hartmann spots.

If the blur spots are thought to be on an x, y grid, then displacement of each blur spot on that grid is a local tilt measurement of each sub aperture's optical wavefront. Using what is called a Fried geometry [3], the x, y focal plane displacements are collected as a column vector and pre multiplied by a reconstruction matrix to give an estimate of the atmospheric turbulence seen at the telescope's aperture. The reconstruction matrix is a regularization design [4, 5], as contrasted with a pseudo inverse design, to minimize excitation of the barely controllable parasitic waffle mode. Figure 4 shows one of many movie frames of optical wavefront Optical Path Difference (OPD).

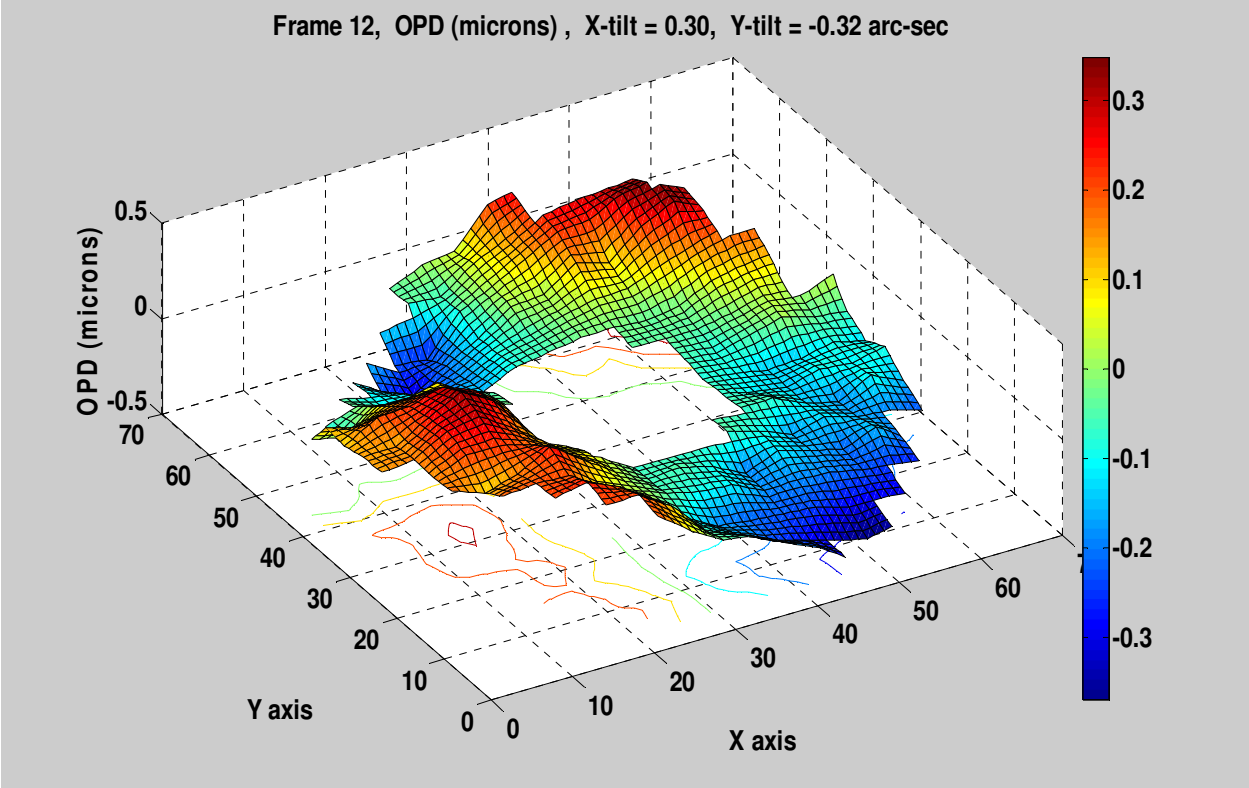

Figure 4 Reconstructed wavefront derived from a 17×17 array of Hartmann spots. The center wavefront can not be reconstructed because its subapertures are in the shadow of the telescope's secondary mirror. The bar graph on the right shows a peak-to-peak OPD of about 0.5 microns, i.e., one wave of aberration of 0.5 micron light.

Conclusion

This paper gives a design for a Shack Hartmann sensor attached to a telescope that is used to measure atmospheric turbulence. The optical beam train is first described, followed by a subaperture discussion of how the number of subapertures are derived. It is seen that there is a tradeoff between the sensor's photon sensitivity and its fidelity of wavefront measurement. Finally, designs for wavefront sensors using different lenslet arrays are compared in a table, and a best is selected.

The uses of the Shack Hartmann sensor are several [6, 7]. One is to compute instantaneous ro more accurately. Another is to find the velocity of the atmospheric aberrations as they traverse the telescope aperture. A third is to identify the presence of multiple turbulence layers in the atmosphere. A fourth is to identify and quantify centroid anisoplanatism [8] by making a power spectrum plot of Zernike decomposition coefficients [9]. A fifth is to better synthesize adaptive optics design simulations by using actual turbulence measurements, as contrasted with the usual approach of using Kolmogorov phase screens with statistics of presumed atmospheric turbulence.

References

[1] D. L. Fried, “Statistics of a geometric representation of wavefront distortion”, J. Opt. Soc. Am. Vol. 56, pp 1372-1379.

[2] Anthony E. Eiegman, Lasers, Chapt. 15, “Ray Optics and Ray Matrices”, University Science Books, 1986

[3] John W Hardy, Adaptive Optics for Astronomical Telescopes, Oxford University Press, 1998

[4] Donald Gavel, “Suppressing Anomalous Localized Waffle Behavior in Least Squares Wavefront Reconstructors” , Proc. SPIE, Vol. 4839, pp 972-980.

[5] W.H. Press, S.A. Teukolsky, W.T. Vetterling, B.P. Flannery, Numerical Recipes, The Art of Scientific Computation, 3rd ed., Section 19.4.1, “The Inverse Problem with Zeroth-Order Regularization”, Cambridge University Press, 2007.

[6] T.J. Brennan, D.C. Mann, “Estimation of Optical Turbulence Characteristics from Shack Hartmann Wavefront Sensor Measurements”, Proc. SPIE, Vol. 7816, Advanced Wavefront Control: Methods, Devices, and Applications VIII, 7781602, August 12, 2010.

[7] T. J. Brennan, “Turbulence Characterization with a Shack-Hartmann Sensor”, SPIE Newsroom, Dec. 14, 2010.

[8] H. T. Yura and M. T. Tavis, “Centroid Anisoplanatism”, JOSA Vol. 2, No. 5, May 1985, pp 765-773.

[9] C. B. Hogge and R. R. Butts, “Frequency Spectra for the Geometric Representation of Wavefront Distortions Due to Atmospheric Turbulence”, IEEE Trans on Antennas and Propagation, Vol. AP-24, No. 2, March 1976, pp 144-154.